Article

Hydrogenative ring-rearrangement of bio-based furanic aldehydes to cyclopentanone compounds over Pd/pyrochlore by introducing oxygen vacancies

Qiang Deng, Rui Gao, Xiang Li, Jun Wang, Zheling Zeng, Ji-Jun Zou, and Shuguang Deng

ACS Catal., **Just Accepted Manuscript** • DOI: 10.1021/acscatal.0c01666 • Publication Date (Web): 10 Jun 2020

Hydrogenative ring-rearrangement of bio-based furanic aldehydes to cyclopentanone compounds over Pd/pyrochlore by introducing oxygen vacancies

Qiang Deng[a]*, Rui Gao[a], Xiang Li[a], Jun Wang[a], Zheling Zeng[a], Ji-Jun Zou[b], Shuguang Deng[c]*

a Key Laboratory of Poyang Lake Environment and Resource Utilization (Nanchang University) Ministry of Education, School of Resource, Environmental and Chemical Engineering, Nanchang University, Nanchang 330031, PR China

b Key Laboratory for Green Chemical Technology of the Ministry of education, School of Chemical Engineering and Technology, Tianjin University; Collaborative Innovative Center of Chemical Science and Engineering (Tianjin), No.92 Weijin Road, Tianjin 300072, China

c School for Engineering of Matter, Transport and Energy, Arizona State University, 551 E. Tyler Mall, Tempe, AZ 85287, USA

*Corresponding Author. E-mail: dengqiang@ncu.edu.cn (Qiang Deng); Shuguang.Deng@asu.edu (Shuguang Deng).

KEYWORDS: hydrogenative ring-rearrangement; furanic aldehydes; Pd/pyrochlore; Lewis acidity; oxygen vacancy

ABSTRACT: Upgrading furanic aldehydes (such as furfural or 5-hydroxymethyl furfural) to cyclopentanone compounds (such as cyclopentanone or 3-hydroxymethyl cyclopentanone) is of great significance for the synthesis of high-value chemicals and biomass utilization. Developing an efficient reduced metal/acidic support with Lewis acidity is the key to facilitating the carbonyl hydrogenation and hydrolysis steps in the hydrogenative ring-rearrangement reaction. Herein, three pure Lewis acidic pyrochlore supports of the form $A_2B_2O_7$ ($La_2Sn_2O_7$, $Y_2Sn_2O_7$, $Y_2(Sn_{0.7}Ce_{0.3})_2O_{7-\delta}$) with the same crystal structures and different metals are synthesized. The Lewis acidity and the surface properties of the pyrochlore can be tuned by inserting different kinds of A and B site metals. After impregnation, Pd nanoparticles with appropriate particle sizes are uniformly loaded on the surface of pyrochlore. For the reaction of the furanic aldehydes, all of these pyrochlore-based catalysts exhibit hydrogenation and hydrolysis rates that are both faster than those of traditional support-based catalysts due to the oxygen vacancy and pure Lewis acidity of the support. Among these pyrochlore-based catalysts, $Pd/Y_2Sn_2O_7$ exhibits activity and selectivity that are higher than those of $Pd/La_2Sn_2O_7$. Moreover, the $Y_2Sn_2O_7$-based catalyst partially substituted by Ce^{3+} ions at the B site is more efficient, with the highest cyclopentanone yield and 3-hydroxymethyl cyclopentanone yield of 95.0% and 92.5%, respectively. Furthermore, the catalyst can still maintain an effective activity and stability after 4 runs. This study not only presents an efficient bio-based route for the production of cyclopentanone compounds but also focuses on the acid catalytic performance of pyrochlore based on its pure Lewis acidity.

Introduction

Upgrading renewable biomass to high-valued fine chemicals is a feasible pathway for achieving a sustainable resource-based economy. Lignocellulose is the most abundant bio-based organic matter, which can be continuously hydrolyzed, dehydrated and generated furanic aldehydes (e.g., furfural (FFA) or 5-hydroxymethyl furfural (HMF)) [1,2]. These furanic aldehydes have been considered as bio-based platform compounds for the preparation of various fine chemicals, such as linear alcohols, 5-furancarboxylic acid, tetrahydrofuran, 2,5-furandicarboxylic acid, 2-methylfuran, 2,5-dimethylfuran, 2,5-dihydroxymethyltetrahydrofuran, cyclopentanone (CPO), 3-hydroxymethyl cyclopentanone (HCPN) [3-10]. Among these fine chemicals, cyclopentanone compounds (e.g., CPO, HCPN) are important building blocks for resins, lysine, vitamins, lubricating oils, and high-density biofuels [11,12], because of the reactivity of hydroxyl and carbonyl groups. At present, CPO is mainly prepared from fossil-derived adipic acid [13]. However, HCPN has not been commercially synthesized yet. Hence, the route of synthesizing cyclopentanone compounds from bio-based furanic aldehydes is promising to provide a sustainable pathway for fine chemicals and to efficiently utilize biomass resources.

The synthesis of cyclopentanone compounds from furanic aldehydes is occurred by continuous carbonyl group hydrogenation, furan ring rearrangement, hydrogenation and dehydration steps. Usually, the reaction is conducted in aqueous solutions (140-190 °C, 2.0-8.0 MPa H_2 pressure) under a reduced metal-supported solid acid catalyst [14]. Currently, various acidic metal oxides (such as TiO_2 and Nb_2O_5), zeolites (such as Hβ, HZSM-5, and SBA-15), metal-organic frameworks (such as Cr-MIL-101 and Cu-MOF) and carbon materials are used as supports for the reaction.[9,10, 15-22] Usually, catalysts with non-acidic support (such as carbon) need a higher reaction temperature and hydrogen pressure because of their weak catalytic ability in the hydrolysis of the hydrogenated product of furfural aldehydes (i.e., 2,5-bis(hydroxymethyl)furan and furfuryl alcohol). It is widely accepted that the type of acidity has an important effect on the reaction. A Lewis acid promotes the synthesis of the target product by ring-opening and intramolecular aldol reactions, and a Brønsted acid easily triggers the generation of macromolecular humins via the intermolecular coupling reaction of active intermediates [23]. These traditional supports with Lewis and Brønsted acid character exhibit an

unsatisfactory catalytic effect on the reactions because of the generation of low-value humins. Recently, we reported some noble metals supported on a metal-organic framework exhibiting pure Lewis acidity that produced a considerable yield of the target product for the reaction [10, 24, 25]. The type of noble metal (i.e., Pd, Pt, Ru, and Au) is optimized, and the Pd nanoparticles exhibit an excellent catalytic performance due to their excellent C=O hydrogenation ability. However, the MOF support is usually unstable under the reaction conditions.

Pyrochlore (format as $A_2B_2O_7$ or $A_2B_2O_6O'$) is ternary metal oxides with a Fm3m space group and cubic unit cell. It is a defective fluorite-type crystal structure (format as B_4O_8), where the B cation is coordinated by eight oxygen ions (Figure 1A). When half of the eight-coordinated B cation (a large radius, typically trivalent rare earth elements) is replaced by six-coordinated A cation (a small radius, usually a tetravalent transition metal elements), the topological structure is transformed from fluorite to pyrochlore [26]. O' and O anions are sited at the 8b and 48f sites with mm and 43m site symmetries, respectively. The A and B metal cations are sited at the 16c and 16d sites respectively, both with 3m site symmetry. The 48f oxygen anions are linked to two A and two B cations, and the 8b oxygen anions are linked to four B cations. In the pyrochlore structure, the 8a oxygen anions are vacant (Figure 1B). Besides the natural oxygen vacancies, the oxygen vacancies can be further generated when the B-site cation is isomorphically substituted by another C metal cation with a lower valence based on the principle of electroneutrality (Figure 1C) [27-29]. In the field of photocatalysis and electrocatalysis, these surface oxygen defects can change the valence state of the metal cation and build a hole in the band structure, leading to a rapid oxygen generation rate for the oxygen evolution reaction [30-35] and photocatalytic water splitting [36]. In contrast, in the field of thermocatalysis, pyrochlore is rarely reported. Currently, pyrochlore is mainly used in the dry reforming of methane [37], the oxidative coupling of methane [38], ethanol steam reforming [39], the catalytic transformation of ethanol into acetone [40], water gas shift reactions [41], and the catalytic reforming of liquid fuels into synthesis gas [42]. These oxygen vacancies are favorable for these reactions involving oxygen-containing compounds. However, these reactions are oxidation-reduction reactions. The pyrochlore has not been reported in the field of acid reactions, nor has it been mentioned in complicated biomass conversion reactions, including acid catalysis and reduced metal catalysis.

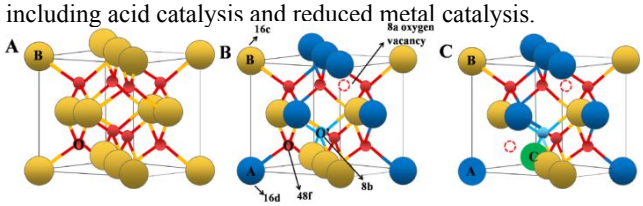

Figure 1. One-eighth of the unit cell of (A) fluorite (B_4O_8), (B) pyrochlore ($A_2B_2O_7$) and (C) B-site substituted pyrochlore ($A_2(B_xC_{1-x})_2O_{7-\delta}$). The substitution of B^{4+} with C cation of low valence states results in a lattice vacancy of oxygen.

Herein, a class of pyrochlore-supported Pd nanoparticle bifunctional catalysts with pure Lewis acidity is prepared for the production of cyclopentanone compounds. The pure Lewis acidity is provided by the coordinated unsaturated metal cation. Meanwhile, the acidity and specific surface area of these catalysts can be controlled by adjusting the kind of A and B site cations. Compared with traditional supported catalysts (Pd/Hβ, Pd/TiO_2, and Pd/Nb_2O_5), the Pd/pyrochlore exhibits a higher catalytic performance because of the strong Lewis acidity, high Pd particle dispersion, and great accessibility of the active sites. Among these Pd/pyrochlore catalysts, $Pd/Y_2(Sn_{0.7}Ce_{0.3})_2O_{7-\delta}$ possesses the best catalytic performance, with the complete conversion of furanic aldehydes, achieving selectivity of cyclopentanone compounds of greater than 91%. Moreover, the catalyst exhibits a stable recycled performance.

Experimental

Materials

Furfural, ammonia, sodium stannate trihydrate ($Na_2SnO_3\cdot3H_2O$), lanthanum nitrate hexahydrate ($La(NO_3)_3\cdot6H_2O$), yttrium nitrate hexahydrate ($Y(NO_3)_3\cdot6H_2O$), cerium nitrate hexahydrate ($Ce(NO_3)_3\cdot6H_2O$), sodium dihydrogen phosphate (NaH_2PO_4), palladium chloride ($PdCl_2$), and sodium carbonate (Na_2CO_3) were supplied by Sinopharm Chemical Reagent Company. Acetone was obtained from the Aladdin Reagent Company. 5-Hydroxymethyl furfural (99%) and TiO_2 (Degussa P25) power were purchased from Beijing Coupling Technology Company. Nano Nb_2O_5 was supplied by Shanghai Chaoqin New Material Technology Company. The Hβ (SiO_2/Al_2O_3 = 25) was obtained from Tianjin Nankai Catalysts Company, and calcined in air for 6 h at 550 °C. Other chemicals were directly used without further treatment.

Preparation of the pyrochlore support

$La_2Sn_2O_7$, $Y_2Sn_2O_7$ and Ce-doped $Y_2Sn_2O_7$ are synthesized by a hydrothermal method. For $La_2Sn_2O_7$ and $Y_2Sn_2O_7$, 8.70 g of $La(NO_3)_3\cdot3H_2O$ (or 7.70 g of $Y(NO_3)_3\cdot6H_2O$), 5.40 g of $Na_2SnO_3\cdot3H_2O$, and 80 mL of water were mixed and then adjusted the pH of 9.0 via ammonium hydroxide. Subsequently, the mixture was added to a 100 mL Teflon-lined autoclave and heated at 200 °C for 24 h. The resultant solid was obtained by filtration, washed by water, dried overnight at 150 °C, and then calcined at 800 °C for 6 h in an air atmosphere. For Ce-doped $Y_2Sn_2O_7$, 2.17 g of $Ce(NO_3)_2\cdot6H_2O$, 7.70 g of $Y(NO_3)_3\cdot6H_2O$, 5.40 g of $Na_2SnO_3\cdot3H_2O$, and 70 mL of water were mixed, adjusted to a pH of 9.0 via ammonium hydroxide, and heated at 200 °C for 24 h. The synthesized $Y_2(Sn_{0.7}Ce_{0.3})_2O_{7-\delta}$ was obtained by filtration, washed, dried, and calcined using the same process used to prepare $La_2Sn_2O_7$ and $Y_2Sn_2O_7$. The element analysis shows that the molar ratio of Y:Sn:Ce is 1:0.7:0.3, which is consistent with the molar ratio of the three metal precursors. The Ce-doped $Y_2Sn_2O_7$ compound is denoted as $Y_2(Sn_{0.7}Ce_{0.3})_2O_{7-\delta}$.

Preparation of the Pd/Pyrochlore catalysts

A $PdCl_2$ solution was impregnated onto the pyrochlore supports via an incipient method. Typically, 1 g of pyrochlore, a certain amount of $PdCl_2$, and 10 mL of water were thoroughly mixed, and the mixture was heated at 80 °C, dried overnight at 110 °C and calcined at 400 °C for 4 h in an air atmosphere. If not mentioned, the $PdCl_2$ content is 0.88 g, and the Pd content on the support surface is 5.0wt%, which is proved by the element analysis. As a comparison, the TiO_2-,

Nb_2O_5-, Hβ-supported catalysts are synthesized via the same process.

Catalyst characterizations

The X-ray diffraction (XRD) was determined by a Panalytical Empyrean diffractometer with a Cu target and Cu-Kα radiation. The X-ray photoemission spectroscopy (XPS) was obtained by an ESCALAB 250Xi with a monochromatic Al anode X-ray gun. The morphology and particle size of the samples were determined using a JEM-2100 transmission electron microscope (TEM). The pore textural properties and the specific surface areas were obtained by performing N_2 adsorption-desorption at -196 °C on an ASAP 2046 surface analyzer. The elemental analysis was carried out on an OPTIMA 5300DV inductively coupled plasma-atomic emission spectrometer. The acid-base properties were characterized by determining the temperature-programmed desorption of ammonia (NH_3-TPD) and carbon dioxide (CO_2-TPD) on a HUASI DAS-7200 instrument. Temperature-programmed reduction (H_2-TPR) were performed on a Micromeritics AutoChem II 2920. The acid type was analyzed by performing pyridine-adsorbed infrared spectroscopy using a Bruker VERTEX 70 spectrometer. Catalyst was tabled to wafer (10 mg/cm^2), degassed and dewatered under vacuum at 200 °C for 1 h, and the pyridine adsorption was performed at 60 °C for 30 min. Then, the temperature gradually increased to 150 °C and 250 °C, and the spectra was recorded. The signal detected at 150 °C and 250 °C was attributed to total acid sites and strong acid sites, respectively.

Catalytic reactions

Typically, 10.4 mmol of furanic aldehydes, 40 mL of water, and 0.1 g of catalyst were added into a 100 mL stainless-steel autoclave from Anhui Kemi Machinery Technology Co., Ltd.. The hydrogen was purged to replace the air for 4 times, and kept at a 4.0 MPa hydrogen pressure. Subsequently, the mixture was stirred at a rate of 600 rpm, and heated to 150 °C, and sampled periodically. 1 mL of the resultant product mixtures was removed from the reactor, extracted by 2 mL ethyl acetate, and 20 μL of internal standard substance (N,N-dimethyl formamide) was added. The concentrations of products were analyzed by a Trace 1300 gas chromatograph equipped with a TG-WAXMS capillary column (30 m × 0.32 mm) and a flame ionization detector (FID). The carbon loss was defined as humins.

In situ Attenuated total reflection infrared (ATR-IR) measurements

The ATR-IR spectroscopy was acquired with a Nicolet iS 50 spectrometer installed with a highly sensitive MCT detector and a heating chamber equipped with CaF windows. The ethanol suspension of the catalyst was dropwise added onto the surface of the diamond probe equipped on the instrument and dried at 100 °C. ATR-IR spectra were recorded with averaging 32 scans at the resolution of 2 cm^{-1}. To simulate catalytic reaction conditions, the catalyst was firstly reduced at 150 °C for 1 h in a 5% H_2/Ar flow, and the background spectrum was recorded before adding of the substrate. Subsequently, the liquid furfural was introduced into the surface of the catalyst by bubbling with an Ar gas stream (flow rate of 40 mL/min). The adsorption of furfural was conducted at 150 °C for 30 min, and the Ar gas stream (flow rate of 40 mL/min) was used to remove the physically adsorbed furfural. In situ ATR-IR spectra of the solid-liquid interface was recorded.

Results and discussion

Structural characteristics of the Pd/pyrochlore catalyst

The XRD patterns of the pyrochlore and the corresponding Pd-supported catalysts are displayed in Figure 2A. All of the samples display the intense diffraction peaks typical of the pure $A_2Sn_2O_7$ (A = La, Y) crystalline phase (2θ = 28.7, 33.3, 47.8, and 56.8°), proving that the pyrochlore phase has been successfully synthesized, and the precipitation of a secondary phase did not occur by the simple hydrothermal method. The elemental analysis data exhibit that the A:B site metal molar ratios of $La_2Sn_2O_7$, $Y_2Sn_2O_7$, $Y_2(Sn_{0.7}Ce_{0.3})_2O_{7-\delta}$ (i.e., 1:1.02, 1:0.98, 1:0.97) are close to the expected stoichiometry of pyrochlore (i.e., 1) (Table 1). Meanwhile, $Y_2(Sn_{0.7}Ce_{0.3})_2O_{7-\delta}$ with Sn^{4+}: Ce^{3+} molar ratio of approximately 0.7: 0.3 exhibits a similar XRD pattern with $Y_2Sn_2O_7$, indicating that Sn^{4+} is partially replaced by Ce^{3+}, which will not change the crystal structure of the $Y_2Sn_2O_7$ pyrochlore type. However, as the A-site cation La^{3+} with replaced with Y^{3+} or the B site Sn^{4+} cation is partially doped by Ce^{3+}, the position of the diffraction peaks has shifted to a larger angle, indicating that the lattice parameter of pyrochlore decreases. According to the literature, the ionic radius of La^{3+} and Y^{3+} is 0.106 and 0.09 nm, respectively [43], and a smaller cation leads to smaller lattice parameters. Meanwhile, the Ce^{3+} ion has a larger ionic radius than Sn^{4+} (0.103 vs 0.07 nm). To maintain electrical neutrality, the partial substitution leads to the formation of oxygen vacancies, which also decrease the lattice parameters. Although the Pd content is approximately 5wt% after impregnation, the Cl content is not detected due to the thermal decomposition of $PdCl_2$ during the preparation conditions (400 °C, 4 h)[44]. The XRD patterns of the catalyst are almost the same as those of the corresponding supports, confirming that Pd nanoparticles are well dispersed on the surface. Moreover, the XRD of Pd/TiO_2 and Pd/Nb_2O_5 only show the characteristic peak of anatase TiO_2 and pseudohexagonal Nb_2O_5 crystals, without the characteristic peak of Pd nanoparticles (Figure S1) [45,46].

The N_2 adsorption-desorption isotherms in Figure 2B show that all of the catalysts exhibit IV type isotherms and H3 type hysteresis rings, which indicated the existence of a mesoporous pore structure generated by particle accumulation. Compared with Pd/$La_2Sn_2O_7$, the Y-contained Pd/$Y_2Sn_2O_7$ has a larger specific surface area of 66.7 m^2/g and a larger pore volume of 0.258 cm^3/g (Table 2). After Ce modification, the specific surface area of Pd/$Y_2(Sn_{0.7}Ce_{0.3})_2O_{7-\delta}$ increases to 89.5 m^2/g, while the pore volume decreases to 0.131 cm^3/g. These results indicate that replacing the A and B site metal changes the particle size of pyrochlore. The Pd/TiO_2 and Pd/Nb_2O_5 possess low specific surface areas of 44.6 and 10.6 m$^2\cdot$g^{-1}, pore volumes of 0.321 and 0.028 cm$^3\cdot$g^{-1}, respectively.

Table 1. Element analysis of Pd/pyrochlore.

Samples	Pd content (wt %)	Cl content (wt %)	La content (wt %)	Y content (wt %)	Sn content (wt %)	Ce content (wt %)	Molar ratio of A:B	Molar ratio of Sn:Ce
$Pd/La_2Sn_2O_7$	4.98	-	29.44	-	25.88	-	1: 1.02	-
$Pd/Y_2Sn_2O_7$	4.95	-	-	21.16	27.67	-	1: 0.98	-
$Pd/Y_2(Sn_{0.7}Ce_{0.3})_2O_{7-\delta}$	5.01	-	-	26.51	24.39	11.88	1:0.97	0.7:0.3

Pd/Hβ shows a specific surface area of 510.2 $m^2 \cdot g^{-1}$ and pore volume of 0.503 $cm^3 \cdot g^{-1}$ due to their microporous structure (Figure S2). As shown by TEM, the pyrochlore crystal size of $Pd/La_2Sn_2O_7$ is obviously larger than that of $Pd/Y_2Sn_2O_7$ and $Pd/Y_2(Sn_{0.7}Ce_{0.3})_2O_{7-\delta}$ (Figure 2 C, D, E). The Pd clusters are uniformly and randomly dispersed on the surfaces of all pyrochlore and other supports (i.e., TiO_2, Nb_2O_5, Hβ) in the range of 3-5 nm (Figure S3). The distribution of Pd nanoparticles was further evaluated by H_2-TPR (Figure S4). All Pd supported catalysts have an obvious peak below 100 °C, which has an approximate peak area. These results indicate that Pd is easily reduced and the dispersion degree of Pd is similar in these catalysts. According to the result of H_2-TPR, a peak that appeared above 500 °C is attributed to the reduction of Sn^{4+} of pyrochlore supports[47].

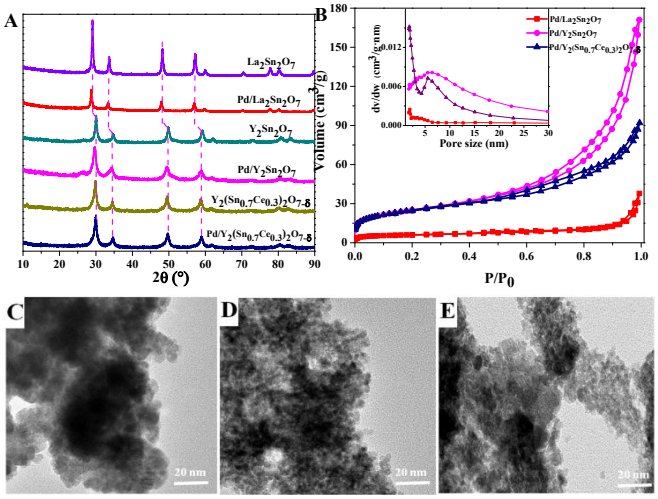

Figure 2. (A) X-ray diffraction patterns of pyrochlore, (B) N_2 adsorption-desorption isotherms and pore diameter distribution of pyrochlore-based catalysts and TEM micrographs of (C) $Pd/La_2Sn_2O_7$, (D) $Pd/Y_2Sn_2O_7$, (E) $Pd/Y_2(Sn_{0.7}Ce_{0.3})_2O_{7-\delta}$.

Table 2. Physicochemical properties of catalysts.

Samples	S_{BET} (m^2/g)	Pore Volume (cm^3/g)	Total Lewis Acid Amount (mmol/g)	Strong Lewis Acid Amount (mmol/g)	Brønsted Acid Amount (mmol/g)	Alkali Amount (mmol/g)
Pd/TiO_2	44.6	0.321	0.006	0.003	0.001	0.008
Pd/Nb_2O_5	10.6	0.028	0.006	0.004	0.001	0.009
Pd/Hβ	510.2	0.503	0.044	0.032	0.151	/
$Pd/La_2Sn_2O_7$	20.9	0.054	0.018	0.009	0.001	0.029
$Pd/Y_2Sn_2O_7$	66.7	0.258	0.041	0.023	0.001	0.033
$Pd/Y_2(Sn_{0.7}Ce_{0.3})_2O_{7-\delta}$	89.5	0.131	0.046	0.032	0.001	0.037

To investigate the influence of the acid-base properties of the catalyst, NH_3 and CO_2-TPD tests were carried out, as shown in Figure 3, Figure S5 and Figure S6. Obviously, the NH_3-TPD result shows that all the pyrochlore-based catalysts exhibit a much higher acid amount than that of the TiO_2- and Nb_2O_5-based catalysts. For the pyrochlore-based sample, two desorption peaks appear at 200 and 400 °C, which was attributed to the acidity of the coordinated unsaturated B-site metal sites, respectively. The acid strength is described by the NH_3-desorbed temperature. Among the Pd/pyrochlore, $Pd/Y_2(Sn_{0.7}Ce_{0.3})_2O_{7-\delta}$ (210, 308 °C) shows a stronger acidity than that of $Pd/La_2Sn_2O_7$ (182, 261 °C) and $Pd/Y_2Sn_2O_7$ (179, 277 °C). Furthermore, CO_2-TPD result in Figure S6 indicates these Pd/pyrochlore possess a large amount of basic site because of the rare earth metals.[38] Subsequently, IR spectra of the in-situ adsorbed pyridine were used to detect the acid types. The acid density of Lewis and Brønsted acidic sites was calculated using the Emeis equation (Table 2, Figure S7) [48]. The pyridine-adsorbed FTIR spectra of the pyrochlore-, TiO_2- and Nb_2O_5-based samples treated at 150 °C exhibit peaks at 1450 cm^{-1} and very weak peaks at 1540 cm^{-1}. This confirms the pure Lewis acidity of the pyrochlore, TiO_2, and Nb_2O_5 supports. On the contrary, in addition to exhibiting Lewis acidity, zeolite Hβ exhibits a considerable Brønsted acidity. Due to the similar topology of three pyrochlore, the acid amount of Pd/pyrochlore is positively correlated with the BET area. Because of the larger specific surface area, more active coordinated metal sites are exposed. In particular, $Pd/Y_2(Sn_{0.7}Ce_{0.3})_2O_{7-\delta}$ exhibits the highest Lewis acid amount of 0.046 mmol/g, as shown in Table 2. Meanwhile, the acid density of strong Lewis acidic sites was calculated based on the signal detected 250 °C. Agreed with the result of NH_3-TPD, the $Pd/Y_2(Sn_{0.7}Ce_{0.3})_2O_{7-\delta}$ shows the highest strong Lewis acid amounts of 0.032 mmol/g (Figure 3B).

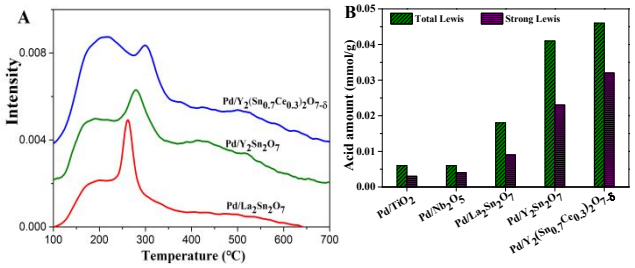

Figure 3. (A) NH_3-TPD profile and (B) Lewis acid amount detected by pyridine-adsorbed FTIR spectra of catalysts.

The surface properties were further investigated by XPS for the catalysts (Figure 4). The Pd 3d XPS spectra of the supported catalyst shows that peaks appear at 335.1 and 340.8 eV (attributed to the $3d_{5/2}$ and $3d_{3/2}$ peaks of Pd(0)) as well as 337.8 and 343.2 eV (ascribed to the $3d_{5/2}$ and $3d_{3/2}$ peaks of

Pd(II)) [49]. Agreed with the result of H_2-TPR, Pd(II) can be in-situ reduced to Pd(0) under the reaction conditions, which is confirmed by the XPS spectrum of the used catalysts (Figure S8) [50]. The weak peak around 200 eV may be ascribed to the trace residue Cl on the catalyst surface. Meanwhile, the XPS peaks of O1s has two peaks (O_I and O_{II}) at 530.0 and 531.7 eV for all pyrochlore-based catalysts [51]. The O_I is attributed to the lattice oxygen, and the O_{II} is attributed to the surface-adsorbed oxygen species on oxygen vacancies. After partial substitution of Sn^{4+} by Ce^{3+}, the O_{II}/O_I peak area ratio of $Pd/Y_2(Sn_{0.7}Ce_{0.3})_2O_{7-\delta}$ is obviously higher than $Pd/Y_2Sn_2O_7$ (0.91 vs 0.71). Combined with the result of NH_3-TPD, the oxygen vacancies are further created and then the B-site cation is isomorphically substituted by another metal cation with a lower valence based on the principle of electroneutrality. Combined with the result of NH_3-TPD and Py-FTIR, the incorporation of Ce^{3+} in the pyrochlore leads to the formation of oxygen vacancies and further exposure of the coordinative-unsaturated Sn^{4+}.

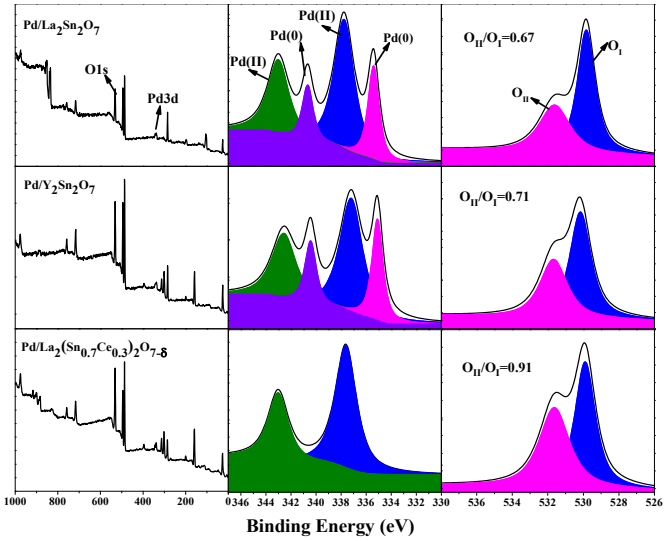

Figure 4. XPS spectra of Pd/pyrochlore.

Hydrogenative ring-rearrangement of furfural

As shown in Figure 5A, the hydrogenative ring-rearrangement of furfural (FFA) to cyclopentanone (CPO) involves a hydrogenation reaction to form furfuryl alcohol (FA), hydrolysis ring-opening reaction to form 2-pentene-1,4-dione (PED), intramolecular aldol reaction to form 4-hydroxy-2-cyclopentenone (HCPEO), then hydrogenation, dehydration reactions to form CPO. A trace amount of PED, HCPEO, and HCPO is detected by GC-MS, indicating that the reactivity of intramolecular aldol and dehydration are fast. Figure 5B, 5C shows the catalytic kinetics under Pd/TiO_2 and $Pd/Y_2Sn_2O_7$ catalysis. A large amount of FFA and FA exhibits that the carbonyl group hydrogenation and hydrolysis reactions are the rate-limiting steps. With increasing reaction time, FA is gradually transformed, and CPO is gradually generated. The concentration of FA intermediate first increased and then decreased. The active carbonyl, furan ring, and hydroxyl groups in FA, intermediates and CPO can easily result in a carbon loss by some intermolecular coupling reactions. Interestingly, some by-products of tetrahydrofurfuryl alcohol (THFA) are created via the furan ring hydrogenation of FA (Figure 5A). Compared with Pd/TiO_2, $Pd/Y_2Sn_2O_7$ possesses three obvious advantages. First, the conversion of FFA is increased from 51.0% to 91.1% within 6 h by the acceleration of the C=O hydrogenation reaction. Secondly, the selectivity of THFA is decreased from 11.0% to 2.0%, and the furan ring hydrogenation reaction is completely inhibited. Thirdly, the selectivity of FA decreased from 8.1% to 5.1% and the selectivity of humins decreased from 14.8% to 1.9%.

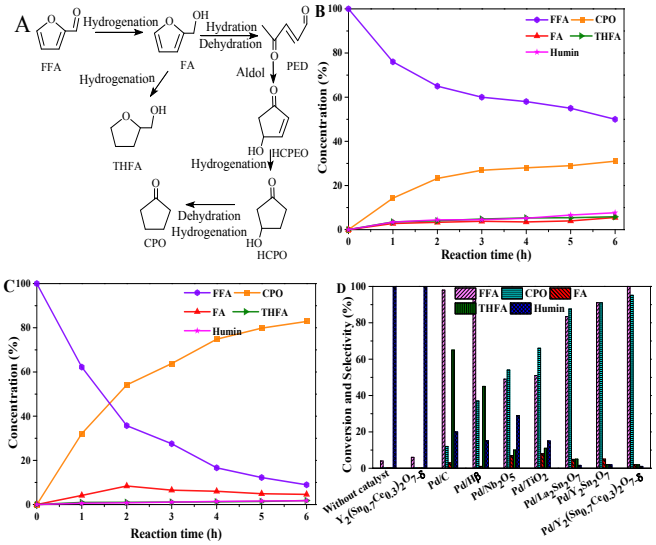

Figure 5. (A) The reaction pathway of FFA reaction; (B), (C) product concentration over Pd/TiO_2 and $Pd/Y_2Sn_2O_7$; (D) catalytic performance of FFA reaction over various catalysts. Reaction conditions: H_2O (40 mL), catalyst (0.1 g), FFA (10.4 mmol), temperature 150 °C, time 6 h, 4.0 MPa H_2 pressure.

Figure 5D further evaluates the catalytic performance of other catalysts. The reaction without catalyst or with only pyrochlore show no FFA conversion and CPO yield, because the hydrogen cannot be activated. Pd/C exhibits a high hydrogenation activity, whereas basically no CPO is generated due to the lack of acid sites. All of the conventional metal oxide-supported Pd catalysts (Pd/TiO_2, Pd/Nb_2O_5, Pd/Hβ) show a mass generation of humins by the Brønsted acidity catalysis. Pd/Nb_2O_5 and Pd/TiO_2 possess a relatively high CPO selectivity, whereas their catalytic activities are low, and a large amount of THFA is generated because of the furan ring hydrogenation reaction. These results indicate that the promotion of C=O hydrogenation and furan ring hydrolysis and inhibition of furan ring hydrogenation are extremely challenging for the selective synthesis of cyclopentanone. All the pyrochlore-based catalysts exhibit a better activity and selectivity than the traditional metal-oxide-based catalysts because the pyrochlore-based catalysts have a large number of oxygen vacancies and a Lewis acidity. Interestingly, among these pyrochlore-based catalysts, the order of the FFA conversion agreed with the amount of oxygen vacancies: $Pd/Y_2(Sn_{0.7}Ce_{0.3})_2O_{7-\delta}$ (99.9%, 0.91) > $Pd/Y_2Sn_2O_7$ (91.1%, 0.71) > $Pd/La_2Sn_2O_7$ (83.4%, 0.67). According to previous work, the strong Lewis acidity is favorable for the hydrolysis of FA[10,24]. Meanwhile, the order of the CPO selectivity agreed with the amount of strong Lewis acid sites: $Pd/Y_2(Sn_{0.7}Ce_{0.3})_2O_{7-\delta}$ (95.1%, 0.032 mmol/g) > $Pd/Y_2Sn_2O_7$ (91.0%, 0.023 mmol/g) > $Pd/La_2Sn_2O_7$ (87.6%, 0.009 mmol/g). The $Pd/Y_2(Sn_{0.7}Ce_{0.3})_2O_{7-\delta}$ catalyst

with the largest amount of oxygen vacancies and strong Lewis acid sites exhibits a satisfactory catalytic performance, with a FFA conversion of 99.9%, CPO selectivity of 95.1% and CPO yield of 95.0%. To further promote the catalytic effect of Pd/pyrochlore, the Pd loading content was optimized, and 5 wt% Pd/pyrochlore produces the highest yield of CPO (Figure S9). The initial reaction solution before and after adding catalyst was neutral with a pH of 7.0. Then, as pH value was adjusted from 7.0 to 5.8 and 4.5 by the weak acidic NaH_2PO_4 (Figure S10), the presence of Brønsted acid in the acidic solution causes carbon loss rather than the generation of CPO [52,53]. Meanwhile, as pH was increased from 7.0 to 10.5 by the basic Na_2CO_3, the ring-opening reaction is completely suppressed and approximately 90% yield of FA and THFA is obtained.

Hydrogenative ring-rearrangement of 5-hydroxymethylfurfural

These catalysts are also used with 5-hydroxymethyl furfural. 5-hydroxymethyl furfural (HMF) can be converted to 1-hydroxy-3-hexene-2,5-dione (HHED) through carbonyl hydrogenation and hydrolysis ring-opening steps similar to those of the furfural reaction (Figure 6A). These intermediates (e.g., 2,5-bis(hydroxymethyl)furan (BHF), HHED) are verified by GC-MS. In contrast to the FA reaction, the large amount of 1-hydroxyl-2,5-hexanedione (HHD) that existed in the reaction mixture shows that 4-hydroxy-4-hydroxymethyl-2-cyclopentanone (HHCPN) has been synthesized from the hydrolyzed intermediate HHED, which occurs during the first hydrogenation step; then, the intramolecular aldol reaction proceeds rather than the first intramolecular aldol reaction, and then hydrogenation occurs in the furfural reaction. In contrast to the results of our previous study catalyzed by MOF, the BHF concentration is very low catalyzed the metal oxide-based catalyst because the hydrolysis reaction is very fast because of the strong Lewis acidity of pyrochlore[10]. The result indicates that the rate-limiting steps in the HMF reaction are the carbonyl hydrogenation and intramolecular aldol reactions. Compared with the intramolecular aldol of PED to HCPEO in the CPO synthesis, the hydroxymethyl group in HHD transfers electrons to the carbonyl group, thus reducing the aldol reactivity [54]. Moreover, the steric hindrance of hydroxymethyl group further makes the synthesis of 3-hydroxymethyl cyclopentanone (HCPN) more difficult. To synthesize HCPN with a high yield, the reaction time was extended to 12 h. Similarly, the excessive hydrogenation and intermolecular C-C coupling reactions produce the THFA and humin by-products. Likewise, the time-dependent product curve indicates that Pd/pyrochlore exhibits a better activity and selectivity than Pd/TiO_2 due to the higher catalytic activity of the carbonyl hydrogenation, hydrolysis, and intramolecular aldol reactions (Figure 6B, C).

Figure 6D also evaluates the catalytic performance of other catalysts. Blank experiment, pure pyrochlore, Pd/C, Pd/TiO_2, Pd/Nb_2O_5 and Pd/Hβ show unsatisfactory catalytic conversion or selectivity. The pyrochlore-based catalysts exhibit a higher activity of HMF and selectivity toward HCPN than traditional support-based catalysts. Likewise, the order of the HMF conversion agreed with the amount of oxygen vacancies: $Pd/Y_2(Sn_{0.7}Ce_{0.3})_2O_{7-\delta}$ (99.9%, 0.91) > $Pd/Y_2Sn_2O_7$ (96.8%, 0.71) > $Pd/La_2Sn_2O_7$ (95.0%, 0.67). Because the rate-limiting aldol condensation reactions are also catalyzed by acids, the selectivity of HCPN also agreed with the order of the strong Lewis acid amount: $Pd/Y_2(Sn_{0.7}Ce_{0.3})_2O_{7-\delta}$ (92.6%, 0.032 mmol/g) > $Pd/Y_2Sn_2O_7$ (76.4%, 0.023 mmol/g) > $Pd/La_2Sn_2O_7$ (60.0%, 0.009 mmol/g). Finally, after 12 h, the conversion over Pd/ $Y_2(Sn_{0.7}Ce_{0.3})_2O_{7-\delta}$ is 99.9%, the selectivity is 92.6%, and the yield is 92.5%. Besides, compared with the result of our previous study catalyzed by a MOF-based catalyst, the stronger acidity of the pyrochlore-based catalyst more easily catalyzes the intramolecular aldol reaction and produces a high yield of HCPN (92.5% vs 82.0%) [10].

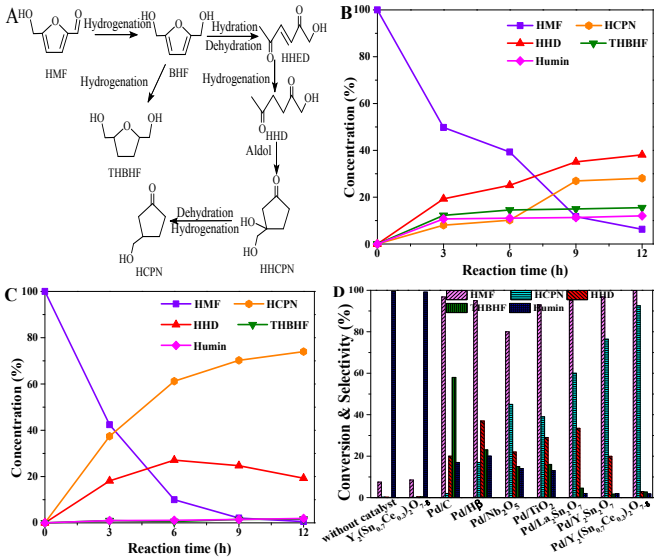

Figure 6. (A) The reaction pathway of HMF reaction; (B), (C) product concentration over Pd/TiO_2 and $Pd/Y_2Sn_2O_7$; (D) catalytic performance of HMF reaction over various catalysts. Reaction conditions: H_2O (40 mL), catalyst (0.1 g), HMF (10.4 mmol), temperature 150 °C, time 12 h, 4.0 MPa H_2 pressure.

Reaction mechanism

To more clearly explain the excellent performance of Pd/pyrochlore, kinetic studies of the FFA hydrogenation step and the FA hydrolysis step are performed. For the hydrogenation step, plotting the $\ln(C/C_0)$ of FFA with respect to time results in a linear relationship, which suggests that the FFA hydrogenation reaction is pseudo-first-order reaction (Figure S11). The hydrogenation kinetics constant is strongly dependent on the amount of oxygen vacancies: $Pd/Y_2(Sn_{0.7}Ce_{0.3})_2O_{7-\delta}$ (1.29 h^{-1}, 0.91) > $Pd/Y_2Sn_2O_7$ (0.41 h^{-1}, 0.71) > $Pd/La_2Sn_2O_7$ (0.30 h^{-1}, 0.67) (Figure 7C). According to previous work, the oxygen vacancy easily selectively fixes and promotes the C=O hydrogenation [51,55]. To understand the mechanism of oxygen vacancy, in-situ attenuated total reflection infrared spectra (ATR-IR) were employed to gain some molecular insight into the adsorption and surface species present on the catalysts under the reaction conditions (Figure 7A). The spectra of the pristine furfural clearly show peaks at 756, 933, 1020 (related to the furan ring) and 1675 cm^{-1} (related to the carbonyl structure) [56]. For Pd/TiO_2, peaks correlated to the furan ring and carbonyl groups have been redshifted about 20 and 30 cm^{-1}. The strong interaction of both furan and carbonyl groups with catalyst suggests flat adsorption of furfural on the Pd/TiO_2 surface [57,58]. In contrast, the spectra of adsorbed furfural on $Pd/Y_2Sn_2O_7$ shows a remarkable red shifted of the carbonyl band (by 20 cm^{-1}),

whereas the furan ring bands remain unchanged compared with the pristine furfural, indicating that Pd/$Y_2Sn_2O_7$ only absorb carbonyl of furfural via a vertical configuration. This adsorption configuration ensures highly selective carbonyl hydrogenation, and the low yield of THFA by-product over all Pd/pyrochlore catalysts. Meanwhile, the adsorption kinetic of furfural from H_2O over $Y_2Sn_2O_7$ and TiO_2 support is studied (Figure 7B, Figure S12). Figure 7B shows the adsorption quality of $Y_2Sn_2O_7$ is obviously higher than TiO_2. The result clearly elucidate the positive influence of the oxygen vacancy.

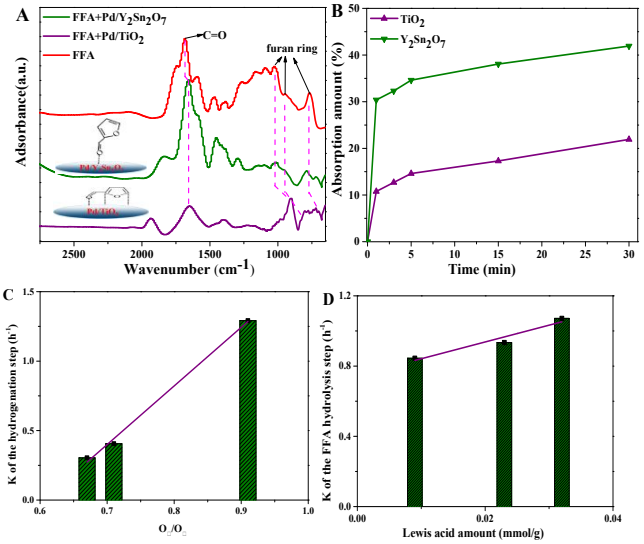

Figure 7. (A) ATR-IR spectra of FFA adsorbed on different catalysts, (B) adsorption kinetics of FFA under $Y_2Sn_2O_7$, and TiO_2, (C) Relationship between oxygen vacancies and hydrogenation rate of FFA; (D) Relationship between acid amount and FA hydrolysis rate. Adsorption conditions: 0.0015 g FFA, 0.05 g catalyst, 30 mL H_2O, temperature 30 °C.

For the FA hydrolysis step, to remove the effect of the FA hydrogenation, the reaction is carried out under nitrogen atmosphere. Likewise, the hydrolysis step of FA has also followed pseudo-first-order kinetics (Figure S13). According to the result of Py-FTIR and NH_3-TPD, the result is that the hydrolysis kinetics constant is dependent on the strong Lewis acid amount of the catalyst: (1.07 h^{-1}, 0.032 mmol/g) > Pd/$Y_2Sn_2O_7$ (0.93 h^{-1}, 0.023 mmol/g) > Pd/$La_2Sn_2O_7$ (0.84 h^{-1}, 0.009 mmol/g) (Figure 7D). More acidic sites are beneficial to the hydrolysis of FA because the Lewis acid sites are more easily accessible to the reactant. Exceptionally, Hβ with a high acid amount exhibits a relatively weak ability to hydrolyze due to their small pore size. Interestingly, in the absence of a catalyst, FA can undergo a slow transformation catalyzed by the hydrogen proton formed by auto-dissociation of water under the reaction temperature (150°C) (Figure S13) [59]. According to the results of the reaction solution with different pH, homogeneous Brønsted acid in the solution is not conducive to ring-rearrangement reaction, but the intermolecular C-C coupling for the formation of humins. The low amount of humins over pyrochlore-based catalysts can be attributed to a large amount of basic site, which can neutralize the in-situ generated hydrogen proton, and guarantee the real pure Lewis acid catalysis. These results show that the great catalytic performance of pyrochlore-based catalysts is ascribable to the high efficiency of the hydrogenation and hydrolysis steps, which are based on Pd/pyrochlore possessing the most oxygen vacancies and Lewis acid amounts, and alkali amounts. To verify whether the conversion of HCPEO from FA proceeds through a two-step of hydrolysis and intramolecular aldol reaction mechanism or a one-step of Piancatteli reaction mechanism, FA is used as the reactant and a certain amount of acetone is added to the reaction system. It is worth mentioning that HCPEO is unstable in water phase, which is easy to aggregate to form humins unless a rapid hydrogenation conversion. PED and HCPEO can be detected by GC-MS when no acetone is added (Figure S14A, Figure S15). After addition of acetone, since the intermolecular aldol reaction rate of PED is faster than that of intramolecular aldol, the aldol product of PED and acetone can be detected instead of HCPEO (Figure S14B, Figure S15). The result demonstrates the two-step mechanism of the ring-rearrangement catalyzed by pyrochlore.

Catalyst stability and reusability

The reusability of the catalyst was determined by the FFA reaction. The spent catalyst was centrifuged, washed by water, dried before the use for next runs. After 4 runs, Pd/$Y_2(Sn_{0.7}Ce_{0.3})_2O_{7-\delta}$ shows a high FFA conversion rate of 99.6%, and the CPO selectivity of 91.2% (Figure 8). The XRD and XPS data of the reused catalysts exhibits that the pyrochlore crystals and oxygen vacancy have been retained (Figure 8B, Figure S8, Table S1). The N_2 adsorption-desorption results indicate the stability of the physical structure (Figure S16, Table S1). This result exhibits that these Pd/pyrochlore catalysts are efficient and stable.

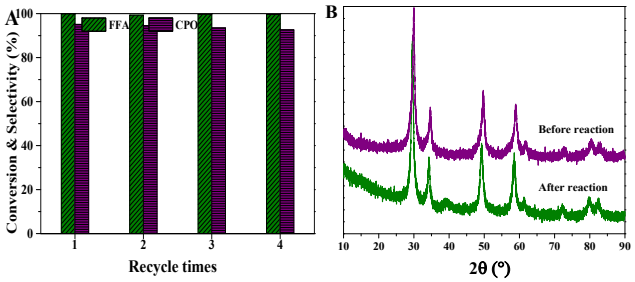

Figure 8. (A) Recycling performance of the Pd/$Y_2(Sn_{0.7}Ce_{0.3})_2O_{7-\delta}$ in FFA reaction. Reaction conditions: H_2O (40 mL), Pd/$Y_2(Sn_{0.7}Ce_{0.3})_2O_{7-\delta}$ (0.1 g), FFA (10.4 mmol), reaction time 6 h, 4.0 MPa H_2 pressure, temperature 150 °C; (B) XRD diffraction patterns of Pd/pyrochlore before and after four catalytic runs.

Conclusion

A series of highly tunable pyrochlore-supported Pd catalysts were developed for the bio-based preparation of cyclopentanone compounds. The oxygen vacancies and Lewis acid amount have a great influence on the hydrogenation and hydrolysis steps, respectively. Various pure Lewis acidities and oxygen vacancies can be tuned by the substitution or partial substitution of the A and B site metal ions in the $A_2B_2O_7$ pyrochlore structure. Compared with the traditionally supported catalysts Pd/Nb_2O_5 and Pd/TiO_2, the pyrochlore catalyst with abundant oxygen vacancies and a strong Lewis acidity exhibits a much higher activity and selectivity. Among the pyrochlore catalysts, the Ce^{3+}-doped $Y_2(Sn_{0.7}Ce_{0.3})_2O_{7-\delta}$ catalyst exhibits the best performance, with cyclopentanone compound yields above 92%, due to the largest specific

surface area, highest oxygen vacancies and highest strong Lewis acid amount. In addition, the pyrochlore catalyst exhibits good stability in the recycling experiment, without any significant pyrochlore structure degradation and Pd leaching. This research provides a highly efficient reaction system for the preparation of cyclopentanone compounds and extends the application prospects of an adjustable pyrochlore catalyst.

Supporting Information

The Supporting Information is available free of charge at https://pubs.acs.org/doi/10.1021/acscatal.xxxxxx.

Some catalyst physicochemical properties and catalytic reaction results, namely, XRD, TEM micrographs, Pyridine-adsorbed FTIR spectra, N_2 adsorption-desorption isotherms, H_2-TPR, NH_3-TPD, CO_2-TPD, XPS spectra, catalytic effect of Pd loading and pH, catalytic kinetics, GC-MS patterns, and UV-vis absorption spectrum (PDF).

Acknowledgments

The authors appreciate the support from the National Natural Science Foundation of China (21878138, 21706112), Postdoctoral Science Foundation of China (2018T110660, 2017M622104) and the start-up funds provided by Nanchang University and Arizona State University.

References

[1] Sudarsanam, P.; Zhong, R.; Van den Bosch, S.; Coman, S. M.; Parvulescu, V. I.; Sels, B. F. Functionalised heterogeneous catalysts for sustainable biomass valorisation. *Chem. Soc. Rev.* **2018**, 47, 8349-8402.

[2] Huber, G. W.; Chheda, J. N.; Barrett, C. J.; Dumesic, J. A. Production of liquid alkanes by aqueous-phase processing of biomass-derived carbohydrates. *Science.* **2005**, 308, 1446.

[3] Hayashi, E.; Yamaguchi, Y.; Kamata, K.; Tsunoda, N.; Kumagai, Y.; Oba, F.; Hara, M. Effect of MnO_2 crystal structure on aerobic oxidation of 5-hydroxymethylfurfural to 2,5-furandicarboxylic acid. *J. Am. Chem. Soc.* **2019**, 141, 890-900.

[4] Motagamwala, A. H.; Won, W.; Sener, C.; Alonso, D. M.; Maravelias, C. T.; Dumesic, J. A. Toward biomass-derived renewable plastics: Production of 2,5-furandicarboxylic acid from fructose. *Sci. Adv.* **2018**, 4, 9722.

[5] Tan, J.; Cui, J.; Zhu, Y.; Cui, X.; Shi, Y.; Yan, W.; Zhao, Y. Complete aqueous hydrogenation of 5-hydroxymethylfurfural at room temperature over bimetallic RuPd/graphene catalyst. *ACS Sustainable Chem. Eng*. **2019**, 7, 10670-10678.

[6] Kumalaputri, A. J.; Bottari, G.; Erne, P. M.; Heeres, H. J.; Barta, K. Tunable and selective conversion of 5-HMF to 2,5-furandimethanol and 2,5-dimethylfuran over copper-doped porous metal oxides. *ChemSusChem.* **2014**, 7, 2266.

[7] Artz, J.; Mallmann, S.; Palkovits, R. Selective aerobic oxidation of HMF to 2,5-diformylfuran on covalent triazine frameworks-supported Ru catalysts. *ChemsusChem.* **2015**, 8, 672-679.

[8] Xiao, B.; Zheng, M.; Li, X.; Pang, J.; Sun, R.; Wang, H.; Pang, X.; Wang, A.; Wang, X.; Zhang, T. Synthesis of 1,6-hexanediol from HMF over double-layered catalysts of Pd/SiO_2 + Ir-ReO_x/SiO_2 in a fixed-bed reactor. *Green Chem.* **2016**, 18, 2175-2184.

[9] Ramos, R.; Grigoropoulos, A.; Perret, N.; Zanella, M.; Katsoulidis, A. P.; Manning, T. D.; Claridge, J. B.; Rosseinsky, M. J. Selective conversion of 5-hydroxymethylfurfural to cyclopentanone derivatives over Cu-Al_2O_3 and Co-Al_2O_3 catalysts in water. *Green Chem. 2017*, 19, 1701-1713.

[10] Li, X.; Deng, Q.; Zhou, S.； Zou, J.; Wang, J.; Wang, R.; Zeng, Z.; Deng, S. Double-metal cyanide-supported Pd catalysts for highly efficient hydrogenative ring-rearrangement of biomass-derived furanic aldehydes to cyclopentanone compounds. *J. Catal.* **2019**, 378, 201-208.

[11] Deng, Q.; Nie, G.; Pan, L.; Zou, J.; Zhang, X.; Wang, L. Highly selective selfcondensation of cyclic ketones using MOF-encapsulating phosphotungstic acid for renewable high-density fuel. *Green Chem.* **2015**, 17, 4473-4481.

[12] Li, H.; Deng, Q.; Chen, H.; Cao, X.; Zheng, J.; Zhong, Y.; Zhang, P.; Wang, J.; Zeng Z.; Deng, S. Benzenesulfonic acid functionalized hydrophobic mesoporous biochar as an efficient catalyst for the production of biofuel. *Appl. Catal. A:Gen.* **2019**, 580, 178-185.

[13] Renz, M.; Ketonization of carboxylic acids by decarboxylation: mechanism and scope. *Eur. J. Org. Chem.* **2005**, 6, 979-988.

[14] Hronec, M.; Fulajtarová, K.; Soták, T. Highly selective rearrangement of furfuryl alcohol to cyclopentanone. *Appl. Catal. B: Environ.* **2014**, 154, 294-300.

[15] Hronec, M.; Fulajtarová, K. Selective transformation of furfural to cyclopentanone. *Catal. Commun.* **2012**, 24, 100-104.

[16] Zhang, G.; Zhu, M.; Zhang, Q.; Liu, Y.; He, H.; Cao, Y. Towards quantitative and scalable transformation of furfural to cyclopentanone with supported gold catalysts. *Green Chem.* **2016**, 18, 2155-2164.

[17] Guo, J.; Xu, G.; Han, Z.; Zhang, Y.; Fu, Y.; Guo, Q. Selective conversion of furfural to cyclopentanone with CuZnAl catalysts. ACS Sustain. *Chem. Eng.* **2014**, 2, 2259–2266.

[18] Li, X.; Deng, J.; Shi, J.; Pan, T.; Yu, C.; Xu, H.; Fu, Y. Selective conversion of furfural to cyclopentanone or cyclopentanol using different preparation methods of Cu-Co catalysts. *Green Chem.* **2015**, 17, 1038-1046.

[19] Wang, Y.; Sang, S.; Zhu, W.; Gao, L.; Xiao, G. CuNi@C catalysts with high activity derived from metal-organic frameworks precursor for conversion of furfural to cyclopentanone. *Chem. Eng. J.* **2016**, 299, 104-111.

[20] Liu, C.; Wei, R.; Geng, G.; Zhou, M.; Gao, L.; Xiao, G. Aqueous phase catalytic hydrogenation of furfural over Ni-bearing hierarchical Y zeolite catalysts synthesized by a facile route. *Fuel Process. Technol.* **2015**, 134, 168–174.

[21] Ohyama, J.; Kanao, R.; Ohira, Y.; Satsuma, A.; The effect of heterogeneous acid-base catalysis on conversion of 5-hydroxymethylfurfural into a cyclopentanone derivative. *Green Chem.* **2016**, 18, 676-680.

[22] Ohyama, J.; Kanao, R.; Esaki, A.; Satsuma, A. Conversion of 5-hydroxymethylfurfural to a cyclopentanone derivative by ring rearrangement over supported Au nanoparticles. *Chem. Commun.* **2014**, 50, 5633-5636.

[23] Swift, T. D.; Nguyen, H.; Erdman, Z.; Kruger, J. S.; Nikolakis, V.; Vlachos, D. G. Tandem Lewis acid/Brønsted acid-catalyzed conversion of carbohydrates to 5-hydroxymethylfurfural using zeolite beta. *J. Catal.* **2016**, 333, 149-161.

[24] Li, X.; Deng, Q.; Zhang, L.; Wang, J.; Wang, R. Zeng, Z.; Deng, S. Highly efficient hydrogenative ring-rearrangement of furanic aldehydes to cyclopentanone compounds catalyzed by noble metals/MIL-MOFs. *Appl. Catal. A: Gen.* **2019**, 575, 152-158.

[25] Deng, Q.; Wen, X.; Zhang, P. Pd/Cu-MOF as a highly efficient catalyst for synthesis of cyclopentanone compounds from biomass-derived furanic aldehydes. *Catal. Commun.* **2019**, 126, 5-9.

[26] Shimakawa, Y.; Kubo Y.; Manako, T. Giant magnetoresistance in $Tl_2Mn_2O_7$ with the pyr ochlore structure. *Nature.* **1996**, 379, 53-55.

[27] Blundred, G. D.; Bridges, C. A.; Rosseinsky, M. J. New oxidation states and defect chemistry in the pyrochlore structure. *Angew. Chem. Int. Ed.* **2004**, 43, 3562-3565.

[28] Hess, N. J.; Begg, B. D.; Conradson, S. D.; McCready, D. E.; Gassman, P. L.; Weber, W. J. Spectroscopic investigations of the structural phase transition in $Gd_2(Ti_{1-y}Zr_y)_2O_7$ Pyrochlores. *J. Phys. Chem. B.* **2002**, 106, 4663-4677.

[29] Pakhare, D.; Shaw, C.; Haynes, D.; Shekhawat, D.; Spivey, J. Effect of reaction temperature on activity of Pt- and Ru-substituted lanthanum zirconate pyrochlores ($La_2Zr_2O_7$) for dry (CO_2) reforming of methane (DRM). *J. CO_2 Util.* **2013**, 1, 37.

[30] Shih, P. C.; Kim, J.; Sun, C. J.; Yang, H. Single-Phase Pyrochlore $Y_2Ir_2O_7$ Electrocatalyst on the activity of oxygen evolution reaction. *ACS Appl. Energy Mater.* **2018**, 1, 3992-3998.
[31] Lebedev, D.; Povia, M.; Waltar, K.; Abdala, P. M.; Castelli, I. E.; Fabbri, E.; Blanco, M. V.; Fedorov, A.; Copéret, C.; Marzari, N.; Schmidt, T. J. Highly active and stable Iridium pyrochlores for oxygen evolution reaction. *Chem. Mater.* **2017**, 29, 5182-5191.
[32] Sun, W.; Liu, J.; Gong, X.; Zaman, W. Q.; Cao, L.; Yang, J. OER activity manipulated by IrO_6 coordination geometry: an insight from pyrochlore iridates. *Sci. Rep.* **2016**, 6, 38429.
[33] Parrondo, J.; George, M.; Capuano, C.; Ayers, K. E.; Ramani, V. Pyrochlore electrocatalysts for efficient alkaline water electrolysis. *J. Mater. Chem. A.* **2015**, 3, 10819-10828.
[34] Kim, M.; Ju, H.; Kim, J. Single crystalline $Bi_2Ru_2O_7$ pyrochlore oxide nanoparticles as efficient bifunctional oxygen electrocatalyst for hybrid Na-air batteries. *Chem. Eng. J.* **2019**,358, 11-19.
[35] Kim, J.; Shih, P. C.; Tsao, K. C.; Pan, Y. T.; Yin, X.; Sun, C. J.; Yang, H. High-performance pyrochlore-type Yttrium ruthenate electrocatalyst for oxygen evolution reaction in acidic media. *J. Am. Chem. Soc.* **2017**, 139, 12076-12083.
[36] Kiss, B.; Didier, C.; Johnson, T.; Manning, T. D.; Dyer, M. S.; Cowan, A. J.; Claridge, J. B.; Darwent, J. R.; Rosseinsky, M. J. Photocatalytic water oxidation by a pyrochlore oxide upon irradiation with visible light: rhodium substitution into yttrium titanate. *Angew. Chem. Int. Ed.* **2014,** 53, 14480-14484.
[37] Pakhare, D.; Schwartz, V.; Abdelsayed, V.; Haynes, D.; Shekhawat, D.; Poston, J.; Spivey, J. Kinetic and mechanistic study of dry (CO_2) reforming of methane over Rh-substituted $La_2Zr_2O_7$ pyrochlores. *J. Catal.* **2014**, 316, 78-92.
[38] Xu, J.; Zhang, Y.; Xu, X.; Fang, X.; Xi, R.; Liu, Y. Zheng, R. Wang, X. Constructing $La_2B_2O_7$ (B = Ti, Zr, Ce) compounds with three typical crystalline phases for the oxidative coupling of methane: the effect of phase structures, superoxide anions, and alkalinity on the reactivity. *ACS Catal.* **2019**, 9, 4030-4045.
[39] Musso, M.; Romero, M.; Faccio, R.; Bussi, J. Catalytic assessment of a Ni-La-Sn ternary metallic system in ethanol steam reforming and the influence of the Sn/La atomic ratio in the catalytic performance. *Catal. Today.* **2019**, DOI: 10.1016/j.cattod.2019.05.043.
[40] Bussi, J.; Parodi, S.; Irigaray, B.; Kieffer, R. Catalytic transformation of ethanol into acetone using copper-pyrochlore catalysts. *Appl. Catal. A:Gen.* **1998**, 172, 117-129.
[41] Playford, H. Y.; Modeshia, D. R.; Barney, E. R.; Hannon, A. C.; Wright, C. S.; Fisher, J. M.; Amieiro-Fonseca, A.; Thompsett, D.; O'Dell, L. A.; Rees, G. J.; Smith, M. E.; Hanna, J. V.; Walton, R. I. Structural characterization and redox catalytic properties of Cerium(IV) pyrochlore oxides. *Chem. Mater.* **2011**, 23, 5464-5473.
[42] Haynes, D. J.; Berry, D. A.; Shekhawat, D.; Spivey, J. J. Catalytic partial oxidation of n-tetradecane using pyrochlores: Effect of Rh and Sr substitution. *Catal. Today* **2008**, 136, 206-213.
[43] Xu, X.; Zhang, R.; Zeng, X.; Han, X.; Li, Y.; Liu, Y.; Wang, X. Effects of La, Ce, and Y oxides on SnO_2 catalysts for CO and CH_4 oxidation. *ChemcatChem* **2013**, 5, 2025-2036.
[44] Wang, H.-F.; Ariga, H.; Dowler, R.; Sterrer, M.; Freund, H.-J. Surface science approach to catalyst preparation-Pd deposition onto thin Fe_3O_4(111) films from $PdCl_2$ precursor. *J. Catal.* **2012**, 286, 1-5.
[45] Yildizhan, M. M.; Sturm S.; Gulgun M. A. Structural and electronic modifications on TiO_2 anatase by Li, K or Nb doping below and above the solubility limit. *J. Mater. Sci.* **2016**, 51, 5912-5923.
[46] Chai, S.-H.; Wang, H.-P.; Liang, Y.; Xu, B.-Q. Sustainable production of acrolein: gas-phase dehydration of glycerol over Nb_2O_5 catalyst. *J. Catal.* **2007**, 250, 342-349.
[47] Ma, Y.; Wang, X.; You, X.; Liu, J.; Tian, J.; Xu, X.; Peng, H.; Liu, W.; Li C.; Zhou, W.; Yuan, P.; Chen, X. Nickel-supported on $La_2Sn_2O_7$ and $La_2Zr_2O_7$ pyrochlores for methane steam reforming: insight into the difference between Tin and Zirconium in the Bsite of the compound. *ChemcatChem* **2014**, 6, 3366-3376.
[48] Emeis, C. A. Determination of integrated molar extinction coefficients for infrared absorption bands of pyridine adsorbed on solid acid catalysts. *J. Catal.* **1993**, 141, 347-354.
[49] Yang, X.; Chen, D.; Liao, S.; Song, H.; Li, Y.; Fu, Z.; Su, Y. High-performance Pd-Au bimetallic catalyst with mesoporous silica nanoparticles as support and its catalysis of cinnamaldehyde hydrogenation. *J. Catal.* **2012**, 291, 36-43.
[50] Hronec, M.; Fulajtárová, K.; Vávra, I.; Soták, T.; Dobročka, E.; Mičušík, M. Carbon supported Pd-Cu catalysts for highly selective rearrangement of furfural to cyclopentanone. *Appl. Catal. B-Environ.* **2016**, 181, 210-219.
[51] Hu, Q.; Yang, L.; Fan, G.; Li, F. Hydrogenation of biomass-derived compounds containing a carbonyl group over a copper-based nanocatalyst: Insight into the origin and influence of surface oxygen vacancies. *J. Catal.* **2016**, 340,184-195.
[52] Yang, Y.; Du, Z.; Huang, Y.; Lu, F.; Wang, F.; Gao, J.; Xu, J. Conversion of furfural into cyclopentanone over Ni-Cu bimetallic catalysts. *Green Chem.* **2013**, 15, 1932-1940.
[53] Ohyama, J.; Ohira, Y.; Satsuma, A. Hydrogenative ring-rearrangement of biomass derived 5-(hydroxymethyl)furfural to 3-(hydroxymethyl)cyclopentanol using combination catalyst systems of Pt/SiO_2 and lanthanoid oxides. *Catal. Sci. Technol.* **2017**, 7, 2947-2953.
[54] Deng, Q.; Xu, J.; Han, P.; Pan, L.; Wang, L.; Zhang, X.; Zou, J. Efficient synthesis of high-density aviation biofuel via solvent-free aldol condensation of cyclic ketones and furanic aldehydes. *Fuel Process. Technol.* **2016**, 148, 361-366.
[55] Zhang, S.; Chang, C. R.; Huang, Z. Q.; Li, J.; Wu, Z.; Ma, Y.; Zhang, Z.; Wang, Yong.; Qu, Y. High catalytic activity and chemoselectivity of sub-nanometric Pd clusters on porous nanorods of CeO_2 for hydrogenation of nitroarenes. *J. Am. Chem. Soc.* **2016**, 138, 2629-2637.
[56] Rogojerov, M.; Keresztury, G.; Jordanov. B. Vibrational spectra of partially oriented molecules having two conformers in nematic and isotropic solutions: furfural and 2-chlorobenzaldehyde. *Spectrochim Acta, Part A.* **2005**, 61, 1661-1670.
[57] Ma, M.; Hou, P.; Cao, J.; Liu, H.; Yan, X.; Xu, X.; Yue, H.; Tian, G.; Feng, S. Simple basic zirconium carbonate: low temperature catalysis for hydrogen transfer of biomass-derived carboxides. *Green Chem.* **2019**, 21, 5969-5979.
[58] Gao, R.; Pan, L.; Wang, H.; Yao, Y.; Zhang, X.; Wang, L.; Zou, J. J. Breaking trade-off between selectivity and activity of Nickel-based hydrogenation catalysts by tuning both steric effect and d-Band center. *Adv. Sci.* **2019**, 6, 1900054.
[59] Li, G.; Li, N.; Zheng, M.; Li, S.; Wang, A.; Cong, Y.; Wang X.; Zhang, T. Industrially scalable and cost-effective synthesis of 1,3-cyclopentanediol with furfuryl alcohol from lignocellulose. *Green Chem.* **2016**, 18, 3607-3613.

Graphic for manuscript